Original Paper

Numerical analysis and measurement of glass flow in a small melting furnace

Toshihiko Hiejima, Hisao Azuma and Masahiko Sawasaki

Department of Aerospace Engineering, Osaka Prefecture University, Sakai, Osaka (Japan)

Hidekazu Hashima, Umihiko Mori, Akio Konishi and Hajimu Wakabayashi

New Glass Research Center, Nihon Yamamura Glass Co., Ltd., Nishinomiya, Hyogo (Japan)

Control of glass flow in a glass tank is a key technology in the glass melting process. The flow and temperature distributions of the glass melt greatly affect the quality of glass products. However, these phenomena have not been well understood due to the difficulty involved in the measurement as a result of the high temperature of the glass melt. A small melting furnace was developed that was heated by electrodes. The glass flow was measured and analyzed by 3-D computer simulation. The numerical results show good agreement with the experimentally measured values. It is shown that it is possible to control the glass convection using a variety of the electric boosting conditions, the heat loss through walls and the charged glass batch. The quality of glass melt was evaluated by analyzing the temperature histories of virtual particles the furnace was charged with. It is found that the temperature of the particles is high and stable near the throat, as shown by the experimental data.

1. Introduction

Recently, the need to enhance the efficiency of glass melting and improve the quality of glass products has increased from the viewpoint of more efficient use of energy [1]. The flow and temperature in a glass melting furnace play an important role in the decomposition, reaction promotion, gas bubble fining, and the homogeneity of glass. The quality of glass products is greatly influenced by the velocity and temperature distributions of glass melting. Understanding and controlling the convection in a glass melting process are very important. Numerical simulation is a very effective method to research the thermal flow in a furnace. Numerical modeling of glass melting has been well described by Viskanta [1]. The majority of the models are two-dimensional. For large furnaces, such models may serve as a useful first approximation. In small to medium glass furnace, however, the wall effects become important, so that two-dimensional models fail to provide a reasonable description of the transport processes occurring within the tank [2 to 5].

In order to evaluate the validity of the numerical simulation of a glass furnace, it is necessary to enhance the comprehension of the physical, chemical and transport processes in glass melting. However, since the environment inside a furnace is severe (high temperature and low velocity), it is very difficult to experimentally determine the actual flow condition in the glass tank. The temperature can be measured using thermocouples or other probes, but the velocity in the glass tank is impossible to measure by ordinary measurement techniques. Almost all measurements performed within the melting furnace have been limited to the flow on the melting surface for a long time. The temperature distribution on the surface of glass has been measured by optical pyrometer [6] and radiation pyrometer, but the surface flow velocity has not been measured.

Although several numerical studies have been performed [2 and 3], velocity measurement in the real glass tank has not been fully explored, and only two methods for the flow velocity measurement have been reported. One method uses a radioactive material [2] and the other uses the pendulum-immersing method [7]. The former method involves measurement of velocity from the radiation of the flow field by mixing isotopes of radioactive substances with the glass batch. But the treatment of radioactive substances is not easy. The latter measures the three-component velocity of the glass flow in a melting furnace. However, since a cooling device protects measurement equipment near the glass surface, the temperature near the surface of melt is reduced in this method. Therefore, a new measurement method that does not affect the measurement values is required.

For the present study, in order to investigate the thermal flow of glass, we developed a small experimental tank, a simplified version of the glass production furnace. We measured the internal temperature distribution, the surface velocity and the internal velocity distribution in the furnace under difficult conditions. Furthermore, the glass flow in the furnace was analyzed via 3-D numerical simulation. We first compared the measured values and the numerical re-

Received 8 August 2002, revised manuscript 7 January 2003.

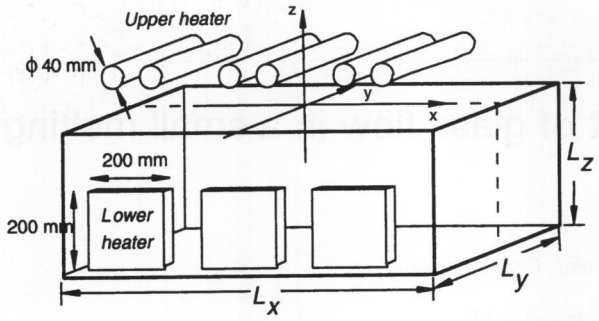

Figure 1. Small glass melting furnace model and coordinate system.

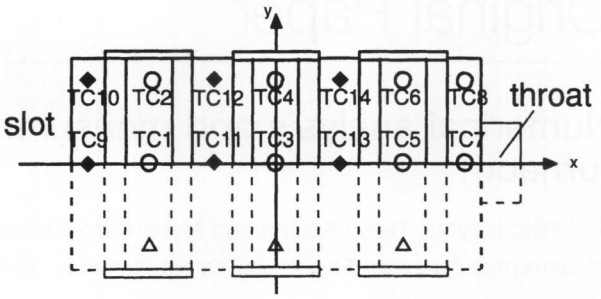

Figure 2. Measurement positions of temperature and velocity in the experimental tank: top view. Three types of temperature measurement were conducted: fixed measurement (○), moving measurement (◆), and measurement of the object for control monitors (△). The velocity was measured at $(x, y) = (0.16, 0)$, $(-0.18, 0)$, (TC13, TC11).

sults for the glass melt. Next, numerical simulations were performed with a view to control of the glass convection. Finally, we evaluated the glass flow in connection to the residence time and temperature histories of virtual particles by dealing with the complex flow case where the injection of glass batch and the glass pull are included.

2. Experimental model

2.1 Small melting furnace

We consider a small melting furnace which is expected to become important for producing several types and small quantities of glass products in the future. Such a glass tank was developed to measure temperature and velocity distributions in the molten glass, including those at the surface. Figure 1 shows a schematic diagram of this glass tank. The sides and bottom of the glass melt are surrounded by refractory walls (electrocast refractory and insulating refractory). The inside length $L_x = 1.0$ m, the inner width $L_y = 0.5$ m and the depth of the melting $L_z = 0.35$ m (the height of electrocast refractory is 0.375 m). Moreover, two types of heat sources are present in the furnace. One is located over the glass melt and the other is placed inside the glass melt. These heat sources are referred to as the upper heater and the lower heater, respectively. We adopted the direct electrified method [8 and 9] for the lower heater. The upper heater is used for indirect heating. Note that this indirect heating method is required for the direct electrified method until the glass comes to a melting state and a degree of conductivity is acquired. Joule heat was generated by the direct electrified method of the lower heater, which utilizes the glass itself as a resistance and depends on the conductivity in the glass melt. The generated heat is almost proportional to the electric power. If the glass temperature becomes higher, the glass resistance will rapidly become smaller and the electric power will increase. The electrode material was molybdenum (Mo), and the electrode form was selected to be a parallel plate ($(0.2 \times 0.2)\ m^2$) in order to make the volume of glass resistance as large as possible. Parallel plate electrodes were placed at three positions in the furnace as shown in figure 1. Three pairs of cylindrical SiC heaters were used as the upper heat source, the diameter of the heater is 0.04 m, and the exothermic part is equal to the inner width of the furnace (0.5 m).

Small melting furnaces can usually be classified as being either the cold-top or hot-top type, according to the surface state of glass. In the former furnace, the surface of glass is covered with the glass batch, and in the latter furnace, the surface of glass is in the melting state. In the present study, although a hot-top type melting furnace was selected in the investigation of the glass flow, in the case of the batch slot and the glass pull the experiments were performed with a partly cold-top state.

In addition, the compositions (in wt%) of the glass used in the present study are as follows: (72.7 SiO_2, 10.8 CaO, 12.4 Na_2O, 2.1 Al_2O_3, 0.2 MgO, 1.3 K_2O).

2.2 Measurement methods for molten glass

The temperature in a glass melt was measured using thermocouples (type B) after a steady state was reached. The thermocouples were sheathed by platinum metal (Pt) in order to prevent corrosion due to the glass. It was thought that the melt and the thermocouples are almost the same temperature and the experimental temperature errors are small. Due to the symmetry at the centerline ($y = 0$), we only measured the temperatures at positions in one half of the glass tank (see figure 2). The thermocouples were placed at 14 positions (TC1 to TC14), as shown in figure 2, and were inserted from the top of the furnace. The temperature of three depths, 0.025 m, 0.175 m, and 0.325 m, below the surface of the melt was measured. Therefore, we were able to measure the temperature at 42 points in the glass flow simultaneously.

We also measured the surface velocity of the glass melt by observing a tracer floating on the surface. Since the tracer appears dark on the surface of melt, we are able to detect the movement of the tracer. We used a small silica refractory cut as the tracer. The movement of the tracer is observed via a CCD camera through a window of the furnace. The camera is protected from the heat by water-cooling, air-cooling and a light trap filter.

In order to measure the flow in a melting tank, we developed a velocity measurement device which was attached to the alumina sphere at the tip of a pendulum. An acrylic pipe of low elasticity was connected to the top of the pendulum, and a strain gauge was attached to the pipe. When the sphere is inserted into the melt, a fluid force working on the sphere is detected by the strain gauge. The measurement accuracy was improved considerably by increasing the sensi-

tivity of bending strain at the instrumental position. As for the effect of the device on the local flow and temperature in the vicinity of the device, the flow is very slow and temperature is not different between the device and the melt because it takes sufficient time for setting and regulating the device. This device can measure only the flow velocities in the x and y directions. The velocity measurement device is located at the positions TC11 and TC13 as shown in figure 2. A detailed description of the velocity measurement method is presented elsewhere [10].

3. Numerical analysis

3.1 Mathematical model and assumptions

The flow in a glass melting furnace involves several complicated physical and chemical processes at high temperature. It is desirable that these processes are simplified without losing a variety of states in the furnace. Therefore, the molten glass is assumed to be an incompressible, homogeneous and Newtonian fluid [2 and 3]. The effect of density variations is important only in terms of buoyancy. All evaporation of species through the glass surface, gas bubble generation, heat dissolution, and the variation of glass composition on the walls are neglected. The governing equations can be expressed as follows using the Navier-Stokes equations and the Boussinesq approximation:

mass equation:

$$\frac{\partial u}{\partial x} + \frac{\partial v}{\partial y} + \frac{\partial w}{\partial z} \equiv 0 , \tag{1}$$

momentum equations:

$$\varrho\left(\frac{\partial u}{\partial t} + u\frac{\partial u}{\partial x} + v\frac{\partial u}{\partial y} + w\frac{\partial u}{\partial z}\right) = -\frac{\partial p}{\partial x} + \frac{\partial}{\partial x}\left(\mu\frac{\partial u}{\partial x}\right) + \frac{\partial}{\partial y}\left(\mu\frac{\partial u}{\partial y}\right) + \frac{\partial}{\partial z}\left(\mu\frac{\partial u}{\partial z}\right),$$

$$\varrho\left(\frac{\partial v}{\partial t} + u\frac{\partial v}{\partial x} + v\frac{\partial v}{\partial y} + w\frac{\partial v}{\partial z}\right) = -\frac{\partial p}{\partial y} + \frac{\partial}{\partial x}\left(\mu\frac{\partial v}{\partial x}\right) + \frac{\partial}{\partial y}\left(\mu\frac{\partial v}{\partial y}\right) + \frac{\partial}{\partial z}\left(\mu\frac{\partial v}{\partial z}\right), \tag{2}$$

$$\varrho\left(\frac{\partial w}{\partial t} + u\frac{\partial w}{\partial x} + v\frac{\partial w}{\partial y} + w\frac{\partial w}{\partial z}\right) = -\frac{\partial p}{\partial z} + \frac{\partial}{\partial x}\left(\mu\frac{\partial w}{\partial x}\right) + \frac{\partial}{\partial y}\left(\mu\frac{\partial w}{\partial y}\right) + \frac{\partial}{\partial z}\left(\mu\frac{\partial w}{\partial z}\right) + \varrho\, g\, \beta(T - T_0),$$

energy equation:

$$\varrho\, C_p\left(\frac{\partial T}{\partial t} + u\frac{\partial T}{\partial x} + v\frac{\partial T}{\partial y} + w\frac{\partial T}{\partial z}\right) = \frac{\partial}{\partial x}\left(\kappa_{\text{eff}}\frac{\partial T}{\partial x}\right) + \frac{\partial}{\partial y}\left(\kappa_{\text{eff}}\frac{\partial T}{\partial y}\right) + \frac{\partial}{\partial z}\left(\kappa_{\text{eff}}\frac{\partial T}{\partial z}\right) + Q_i \tag{3}$$

where (u, v, w) is the velocity vector, ϱ the density evaluated at the reference temperature T_0, T the temperature, p the pressure, g the gravitational acceleration, β the thermal expansion coefficient, and C_p the specific heat. Since the viscosity was determined by the Fulcher correlation [5], we applied it to the experimentally measured value.

$$\ln \mu = -3.409 + \frac{5441}{T - 469.0} . \tag{4}$$

The effective thermal conductivity κ_{eff} can be expressed as the sum of the thermal conductivity κ and the radiation via the Rosseland diffusion approximation [3] if the optical thickness is assumed to be thick.

$$\kappa_{\text{eff}} = \kappa + \frac{16\, n^2\, \gamma}{3\chi_R}\, T^3 . \tag{5}$$

Here, γ is the Stefan-Boltzmann constant, n is the refractive index of the glass, and 3χ is the mean absorption coefficient. Physical properties used in the simulations are demonstrated in table 1.

Next, we estimate the Joule heat Q_i generated by the lower heater. The power source distribution generated through electric boosting within the glass melt is exactly determined by solving Maxwell's equations in the electromagnetic field [5]. Here, we assume that all of the added electric power is converted to Joule heat dissipation. Therefore, the cuboid area (volume $V_h = 0.02\ \text{m}^3$) between parallel electrodes in the glass flow is defined as the distribution of the heat source. The volumetric rate of Joule heat dissipation Q_i in the energy equation can be expressed as

$$Q_i \equiv (\text{electric power})_i / V_h \tag{6}$$

where $i \equiv 1, 2, 3$.

The calorific value transmitted from the upper heater is expressed using the relationship between the radiation energy and the radiation intensity. This radiation is modeled using the distance r from the upper heater (1) to the flow surface (2) and the heater configuration as shown in figure 3.

$$\Delta\dot{Q}_{2,i}^{(k)} = \frac{\Delta\dot{Q}_1^{(k)}}{\pi} \int_{S_1} \frac{\cos\phi_1 \cos\phi_2}{r^2}\, dS_1 dS_2 , \tag{7}$$

Table 1. Physical properties used in the simulations

density	ϱ	2.36×10^3 kg/m^3
thermal expansion coefficient	β	7.43×10^{-5} 1/K
specific heat	C_p	1.55×10^3 J/(kg/K)
thermal conductivity	κ	1.5 W/(m K)
surface tension gradient	$-\frac{\partial\sigma}{\partial T}$	2.07×10^{-5} N/(m K)
viscosity	$\ln\mu = -3.409 + \frac{5441}{T-469.0}$	Pa s
gravitational acceleration	g	9.8 m/s^2
refractive index of the glass [14]	n	1.52
Stefan-Boltzmann constant	γ	5.669×10^{-8} W/(m^2 K^4)
mean absorption coefficient [15]	χ_R	10 m^{-1}

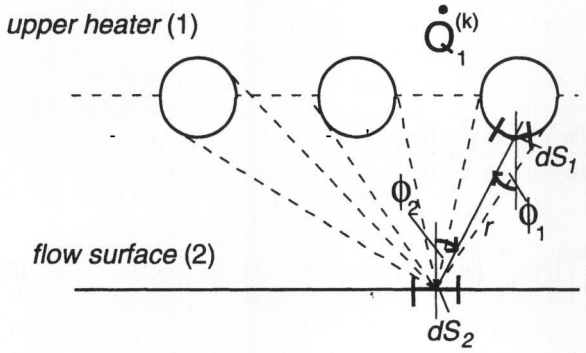

Figure 3. Schematic representation of heat flux estimation on the surface of melt.

$$|q_{rad}| = \sum_k \frac{\Delta\dot{Q}_{2,i}^{(k)}}{\Delta S_2} . \tag{8}$$

The effect of surface tension was neglected in previous studies. The surface tension does not have an effect on the melt in a steady state according to the numerical results, because the temperature gradient of the surface tension σ is much smaller than the viscous force (order 10^{-5} N/(m K)). Although, when there is a local difference temperature in the melt, we consider it has a slight influence on the glass flow. It is known that the surface covered with glass batch has a lower temperature compared to the glass melt. We observed experimentally that the batch was pushed back to the entrance slot side by the flow (namely, Marangoni flow) produced due to the temperature gradient. Consequently, the present study takes the surface tension into consideration.

3.2 Computational domain

The origin of coordinates needed in both the numerical simulation and the experimental measurement positions was set in the center of the melting surface. We defined the direction from the slot to the throat as the x-axis; the horizontal and vertical directions perpendicular to the x-axis were defined as the y-axis and the z-axis, respectively. Since this furnace is symmetrical with respect to the x-axis, only one half of the three-dimensional domain needs to be considered.

3.3 Boundary conditions

The velocity conditions on the wall are nonslip. Although surface deformation is ignored, the surface tension is considered in the velocity conditions. The velocity in the vertical direction is assumed to vanish at the interface. These conditions show the free surface. Temperature boundary conditions were extrapolated from the experimentally measured values near the wall. Here, T_{sw}, T_{fw}, T_{rw} and T_{bw} indicate temperature distributions extrapolated from the planes of the sidewall, front wall, rear wall and bottom wall, respectively. The thermal boundary condition at the glass surface is greatly dominated by radiation [11]. The boundary conditions are summarized as follows:

front wall: $x = 0$; $u = v = w = 0$, $T = T_{fw}$,

$$\frac{\partial P}{\partial x} = \frac{\partial}{\partial x}\left(\mu\frac{\partial u}{\partial x}\right), \tag{9}$$

rear wall: $x = L_x$; $u = v = w \equiv 0$, $T \equiv T_{rw}$,

$$\frac{\partial P}{\partial x} = \frac{\partial}{\partial x}\left(\mu\frac{\partial u}{\partial x}\right), \tag{10}$$

side wall: $y = L_y/2$; $u \equiv v = w \equiv 0$, $T \equiv T_{sw}$,

$$\frac{\partial P}{\partial y} = \frac{\partial}{\partial y}\left(\mu\frac{\partial v}{\partial y}\right), \tag{11}$$

symmetry plane: $y = 0$; $v = 0$,

$$\frac{\partial u}{\partial y} = \frac{\partial w}{\partial y} = \frac{\partial T}{\partial y} = \frac{\partial P}{\partial y} = 0 , \tag{12}$$

bottom wall: $z = -L_z$; $u \equiv v \equiv w \equiv 0$, $T \equiv T_{bw}$,

$$\frac{\partial P}{\partial z} = \frac{\partial}{\partial z}\left(\mu\frac{\partial w}{\partial z}\right) + \varrho\, g\, \beta(T - T_0) , \tag{13}$$

top surface: $z = 0$; $w = 0$,

$$\mu\frac{\partial u}{\partial z} = \frac{\partial\sigma}{\partial T}\frac{\partial T}{\partial x} , \tag{14}$$

$$\mu\frac{\partial v}{\partial z} = \frac{\partial\sigma}{\partial T}\frac{\partial T}{\partial y} ; \tag{15}$$

Table 2. Experimental and numerical conditions

	upper electric power in kW	lower electric power in kW
case A1	6.0, 6.0, 6.0	3.0, 13.0, 3.0
case A2	6.0, 6.0, 6.0	4.5, 12.0, 4.5
case A3	6.0, 6.0, 6.0	6.0, 10.4, 6.0
case A4	6.0, 6.0, 6.0	7.5, 8.0, 7.5
case A5	6.0, 6.0, 6.0	9.0, 4.7, 9.0
case A6	6.0, 6.0, 6.0	5.0, 5.0, 13.2

$$|q_{\mathrm{rad}}| = -\kappa_{\mathrm{eff}}|\nabla T|\,, \tag{16}$$

$$\frac{\partial P}{\partial z} = -\frac{\partial \sigma}{\partial z}\left(\frac{\partial^2 T}{\partial x^2} + \frac{\partial^2 T}{\partial y^2}\right) + \varrho\, g\, \beta (T - T_0)\,. \tag{17}$$

The following equation (18) is also often used for describing the wall condition [3 and 11],

side or bottom wall:

$$-\kappa_{\mathrm{eff}}\frac{\partial T}{\partial \xi} = K(T - T_\alpha) \tag{18}$$

where, K is the overall heat loss coefficient through the refractory walls, T_α is the ambient temperature and ξ is a normal direction to a wall. When we also take into consideration the glass batch and the pull of glass, the conditions obtained are as follows:

inflow: $z = 0$, $-0.45 \leq x \leq -0.25$, $0 \leq y \leq 0.1$; $w = -U_{\mathrm{in}}$, $u = v = 0$, $T = T_{\mathrm{s}}$,

$$\frac{\partial P}{\partial z} = 0\,, \tag{19}$$

outflow: $x = L_x$, $0 \leq y \leq 0.075$, $-L_z \leq z \leq 0.1$; $u = U_{\mathrm{out}}$, $v = w = 0$,

$$\frac{\partial T}{\partial x} = \frac{\partial P}{\partial x} = 0\,. \tag{20}$$

3.4 Numerical method

The numerical scheme used in the present study is the SMAC method [14], which is often used for incompressible thermal flow. The numerical grid points are $41 \times 11 \times 15$. Since the viscosity of glass is very large and the velocities are quite small, the flow in glass melt can be assumed to be laminar. Therefore, the grid numbers are fit for this simulation, because neither a tiered wall nor an electric cylindrical heater exists in the tank. The simulations are performed until the steady state is reached.

4. Results and discussion

4.1 Comparison of experimental and numerical results

In order to compare experimentally measured values to the numerical results, we dealt with the state of a glass furnace without a pull of glass and a batch effect involved in a cullet slot. Experiments were performed under the electric power conditions (cases A1 to A5) shown in table 2. The conditions of the lower heater were controlled so that the middle heater reached 1625 K. All of the electric power of the upper heaters was maintained at approximately 6 kW. Numerical heater conditions were also used in this experiment condition. Equation (2) was applied for boundary conditions. The measuring points within the small melting furnace for temperature are TC1 to TC14 and the points for velocity are TC11 and TC13 as shown in figure 2, respectively.

Figures 4a to h show a comparison of the numerical results and the experimentally measured values. In the centerline ($y = 0$), the surface and the inside of the temperature distributions agreed well with the experimental values. For the surface velocity distribution, the numerical results were slightly larger than the measured values. When part of the furnace wall was opened in order to measure the surface velocity, the surface temperature decreased temporarily, so that the velocity was reduced due to the increased viscosity at the same time. The internal velocity distribution was in agreement with the experimental value. The numerical results firmly captured the return flow due to two dominant circulations and the position of zero velocity. However, these results were not consistent with a deep position, because measurement errors are thought to become large in the vicinity of the bottom wall.

Figure 5 shows the calculated velocity vectors and temperature isosurfaces in the symmetrical plane ($y = 0$). The boundary temperature is estimated by extrapolating the measured values near the wall. Therefore, heat exchange between the walls and the glass flow was almost perfectly insulated. Fundamentally, the dominant flows in each case were two large circulations (primary flows). These glass flows were generated when the rising flow caused by the most powerful heater (e.g. middle) was cooled at the front and rear walls. The vortical center of the circulation was observed to be expanding from the sidewall to the centerline in the X-Z plane. This occurred due to the effect of a circulation (secondary flow) in the Y-Z plane. Thus, the three-dimensional flow exists in a lateral direction due to the effect of the sidewall temperature distribution. The rising flow of case A1 was stronger than that of other cases (A1 to A4), and the churning effect in the furnace was the largest. Moreover, when the difference in electric power was smaller between the lower heaters, the small circulation grew into two large circulations. These two large circulations became one circulation in case A6 of the special electric condition.

As for the measured surface temperature in each case, that of the right side became slightly higher than that of the left side. Since a hot spout existed in the throat side (see also figure 8a), the heat loss through the rear wall was less than that through the front wall. This is due to deviation of the entire velocity vector distribution in figure 5, although the arrangement of electric power was approximately symmetrical. Based on these results, the convection structure of glass melt was clarified by both the experiments and the numerical simulation by changing the electric heater power distribution.

4.2 Convection control of glassy melts

We attempted to control the convection using the heat loss through a wall. In this case, equation (18) was used for the

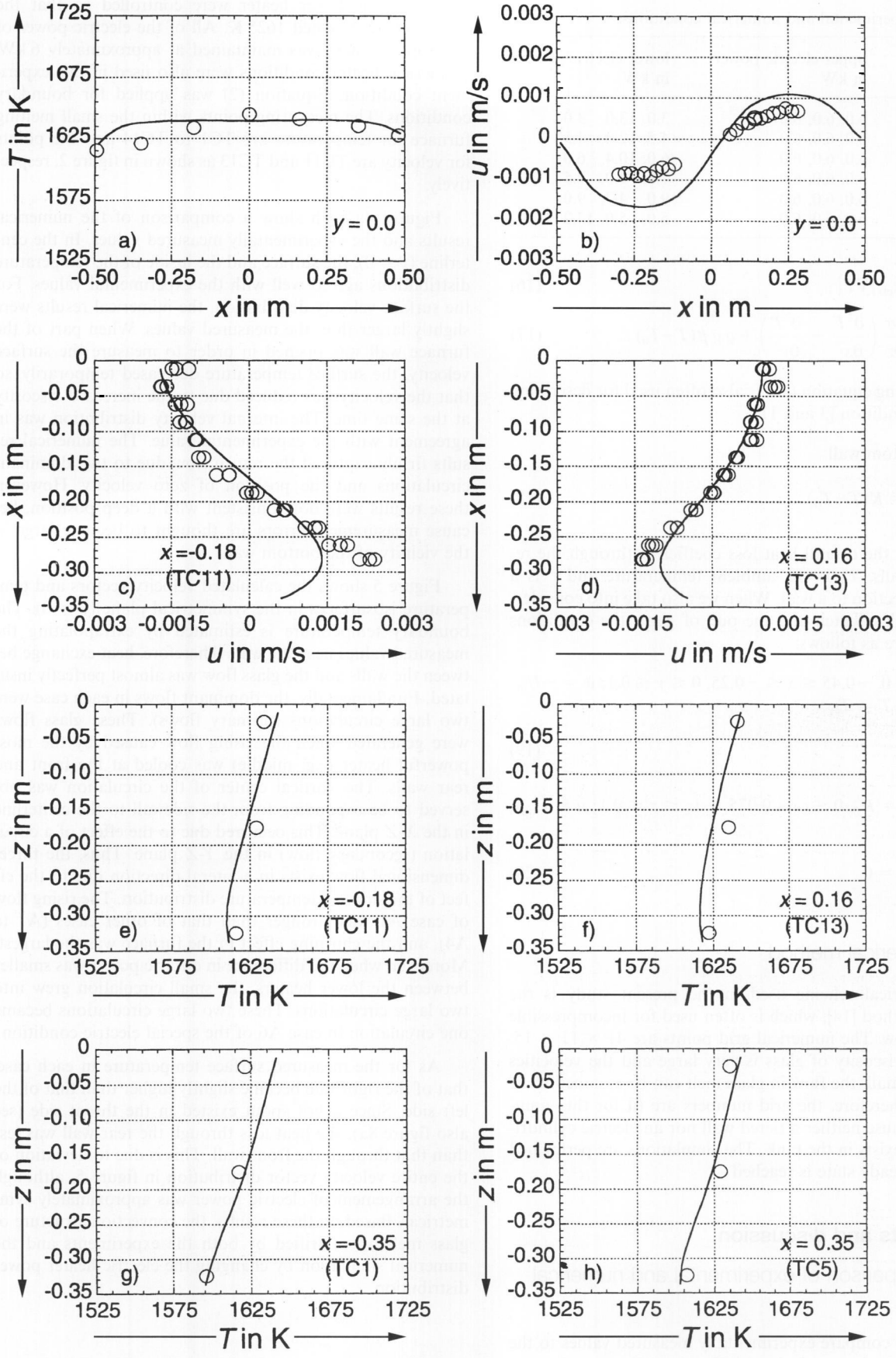

Figures 4a to h. Comparisons of numerical results and experimental measurements for the surface of molten glass and for the inside of molten glass: case A3; temperature distributions: a) $y = 0.0$, e) $x = -0.18$, f) $x = 0.16$, g) $x = -0.35$, h) $x = 0.35$, and velocity distributions: b) $y = 0.0$, c) $x = -0.18$, d) $x = 0.16$.

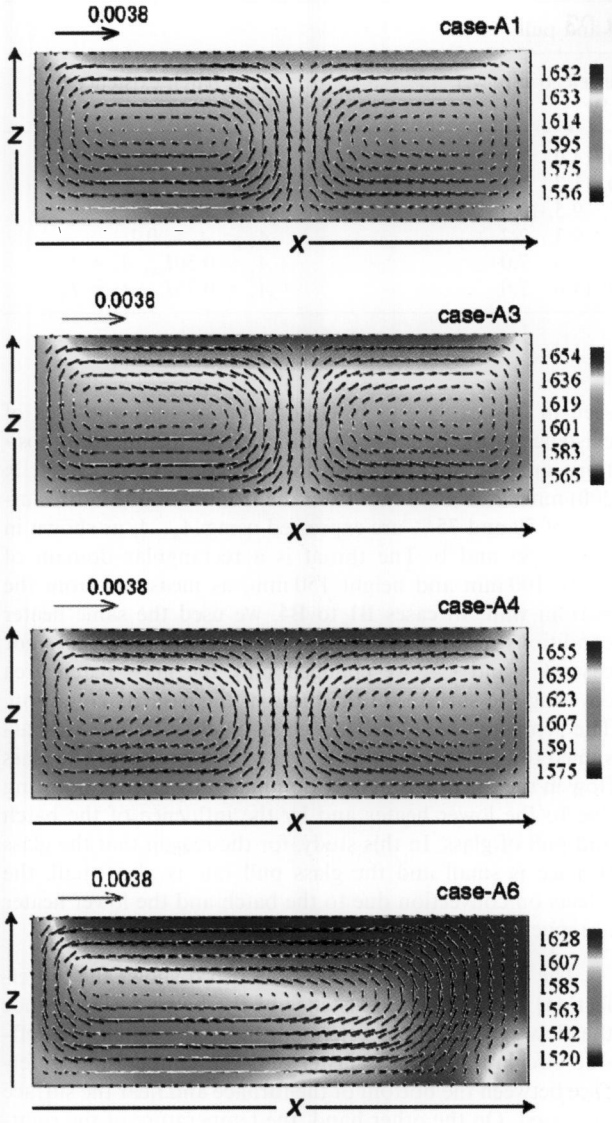

Figure 5. Temperature contour in K and velocity vector in m/s in the glass furnace: cases A1, A3, A4 and A6 at $y = 0$.

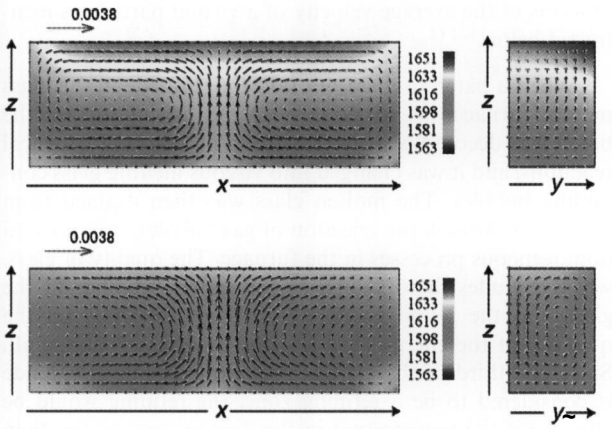

Figure 6. Comparison of case A2 (top) and case A2 for a modified overall heat flux through the sidewall (bottom), at $y = 0$ (left), $x = -0.14$ (right): temperature contour in K and velocity vector in m/s.

boundary conditions. First, we investigated the effect on the small tank when the circulations (secondary flow) become

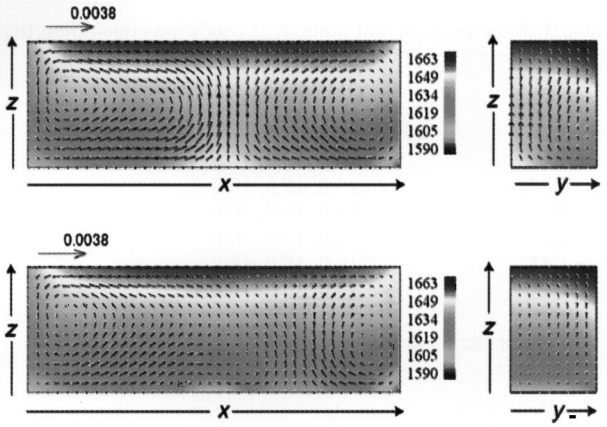

Figure 7. Comparison of case A5 (top) and case A5 for a modified overall heat flux through the bottom wall (bottom), at $y = 0$ (left), $x = 0$ (right): temperature contour in K and velocity vector in m/s.

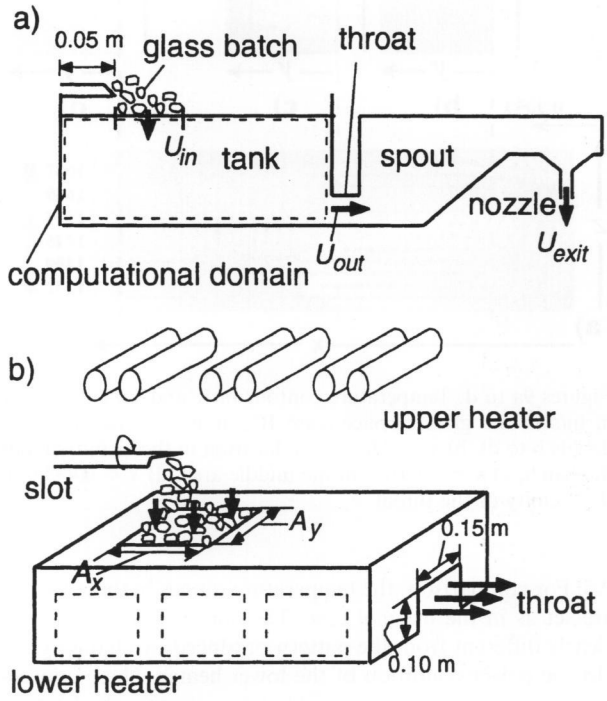

Figures 8a and b. Cross section of the small melting furnace (figure a) and glass batch injection model (figure b).

strong in the *Y-Z* plane. We assumed that the overall heat loss through a sidewall is one-hundred times the overall heat loss coefficient through the refractory wall ($K = 2.585$ W/(m^2 K)). As compared to the original case (case A2), we found that the circulation appeared in the *Y-Z* plane and the rising flow of the *X-Z* plane gradually became stronger (figure 6). This control also enhanced the effect of churning in the furnace. Furthermore, we considered controlling the area of flow using the heat loss through the furnace bottom wall. The overall heat loss through a portion of the bottom wall was assumed to be three-hundred times the overall heat loss coefficient through the refractory wall ($K = 1.775$ W/(m^2 K)). The heat loss domain is an area having the zonal bottom (-0.1 m $\leqq X \leqq 0.1$ m) just under the middle lower heater. Figure 7 shows that the flow in the middle part of the *X-Z* plane was clearly suppressed as compared to case

Table 3. Experimental and numerical conditions: including the batch and pull

	upper electric power in kW	lower electric power in kW	glass batch existence range in m
case B1	10.0, 10.0, 10.0	12.0, 14.0, 7.0	$A_x = A_y = 0.2$
case B2	10.0, 10.0, 10.0	10.0, 11.7, 5.7	$A_x = A_y \equiv 0.2$
case B3	10.0, 10.0, 10.0	8.5, 9.5, 10.0	$A_x = A_y = 0.2$
case B4	10.0, 10.0, 10.0	14.3, 9.3, 2.7	$A_x = A_y \equiv 0.2$
case C1*	10.0, 10.0, 10.0	12.0, 14.0, 7.0	$A_x \equiv 0.50L_x$, $A_y \equiv L_y$
case C2*	10.0, 10.0, 10.0	12.0, 14.0, 7.0	$A_x \equiv 0.75L_x$, $A_y \equiv L_y$

* No experimental data.

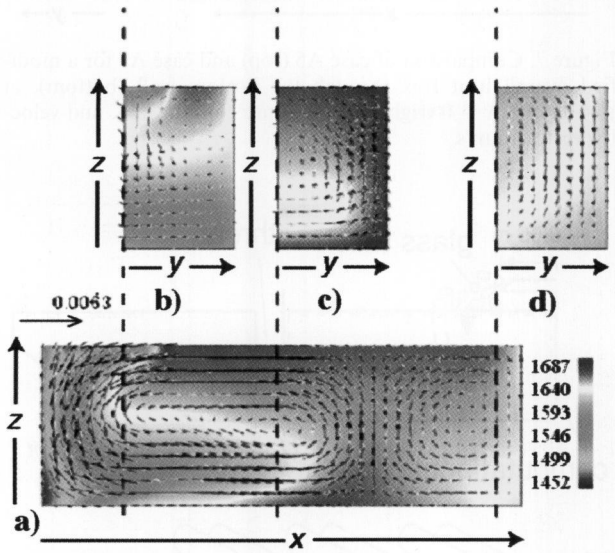

Figures 9a to d. Temperature contour in K and velocity vector in m/s in the glass furnace: case B1, at $y = 0$ (figure a and details b to d), b) $x = -0.36$: in a location in the vicinity under the batch, c) $x = -0.012$: in the middle area, d) $x = 0.4375$: in the vicinity of the throat.

A5. For comparison, the temperature ranges in these figures are set as in the original case. The convection pattern was clearly different from the pattern produced by changing the electric power condition of the lower heater. These convection controls would be realizable by weakening the heat insulation effect, for example by making an outer wall thin or by wall cooling. We demonstrated that simply changing the heat transfer at the wall is effective in providing convection control.

4.3 Evaluation of glass quality

We investigated the effect of the surface batch and the glass pull on the quality of glass products. Numerous effects of the batch have been studied by two-dimensional simulation, e.g. in [13]. The dissolution process of a batch, chemical reactions and bubble reactions were neglected here. The present numerical conditions are summarized in table 3. The amount of injection and pull were comparable to the experimentally measured values 20 kg/h, respectively. The inflow and outflow conditions were set to $U_{in} = \mp(5.88 \times 10^{-5})$ m/s, $U_{out} = (1.57 \times 10^{-4})$ m/s in accordance with mass conservation. The position of injection and the throat area are seen in figures 8a and b. Unfortunately, since the area of existence of the batch was not measured, the injection positions are assumed in three domains as follows: a (200 × 200) mm^2 area at 50 mm from the front wall, the entire surface of 50 and 75 % are expressed using A_x, A_y as shown in figures 8a and b. The throat is a rectangular domain of width 100 mm and height 150 mm, as measured from the bottom wall. In cases B1 to B4, we used the same heater conditions as that used in the small melting furnace. For cases C1 and C2, we changed only the glass batch area covering the surface on the basis of the case B1 condition. The temperature T_s on the glass batch interface was assumed to be 200 K below the average temperature. The glass flow in the furnace is mainly dominated by electric boosting due to the lower heater and by the influence of the batch and pull of glass. In this study, for the reason that the glass furnace is small and the glass pull rate is also small, the effects on convection due to the batch and the lower heater are much larger than those due to glass pull [4 and 5].

The velocity vector in figures 9a to d shows the 'lid effect' [1] caused by the existence of the batch surface. Since the flow was greatly accelerated under the batch, the left-side circulation became faster and the temperature difference between the bottom of the furnace and near the surface increased. On the other hand, the temperature of the right-side circulation was stable, and the velocity was slower than that of the left side. We also confirmed the difference between the left-side circulation and the right-side circulation in terms of the average velocity of a virtual particle as mentioned below.

When a batch of glass put into the slot side in the glass melting furnace was heated through the melting surface, the batch was decomposed by the effects of heat and chemical reactions, and it was changed into viscous melting glass containing bubbles. The molten glass was then drained from the throat through the rejection of gas bubbles, mixture and homogeneous processes in the furnace. The quality of glass, which includes factors such as the bubble number in the glass and the homogeneity of the glass, depends on the quantity of the energy used and the quantity of glass pull. Since one-third of the melting domain near the throat side is considered to be a refining zone, the refining would be effective if the temperature in the domain was higher than that in the rest of domain. Therefore, in order to obtain good-quality glass, the refining zone must be maintained at high temperature and it is essential to prevent an influx of a batch into the throat by controlling the position of a rising flow in melting glass. Moreover, the quality of a glass product is greatly influenced by the residence time and the temperature history of the melt. These could be controlled by

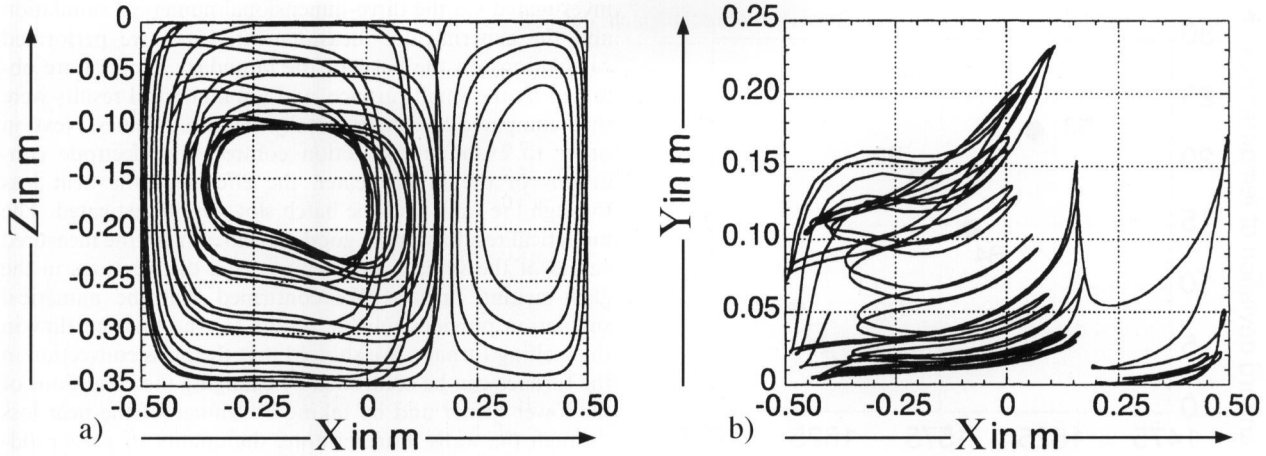

Figures 10a and b. Trajectory of a virtual glass particle in the $X-Z$ plane (figure a) and $X-Y$ plane (figure b): case B1.

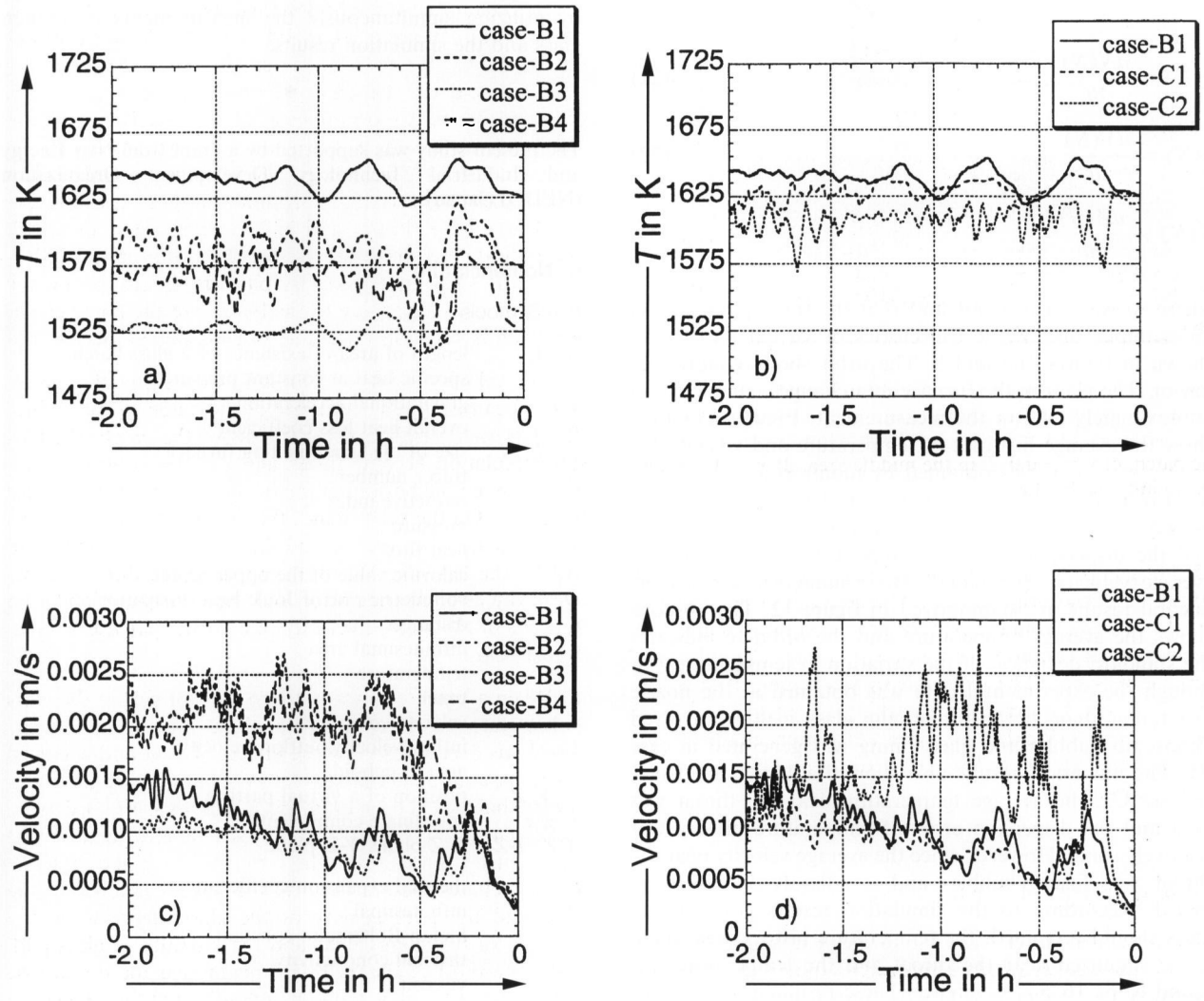

Figures 11a to d. Average temperature history and velocity history of virtual particles near the throat considering the batch and pull of glass; a) temperature histories, cases B1 to B4, b) temperature histories, cases B1, C1 and C2, c) velocity histories, cases B1 to B4, d) velocity histories, cases B1, C1 and C2.

the circulation patterns and the temperature distribution in the melting furnace. We evaluated these via virtual glass particles positioned at the injection slot domain [3]. The position (X, Y, Z) and temperature of the virtual particles were monitored using the numerical data of a steady state (u, v, w, T) as demonstrated in equations (21 to 23).

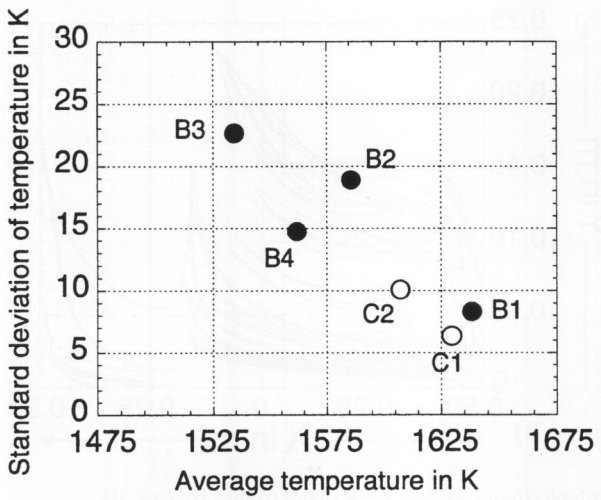

Figure 12. Quality evaluation of the produced glass.

$$u(N) = \frac{dN(N)}{dt}, \tag{21}$$

$$v(N) = \frac{dY(N)}{dt}, \tag{22}$$

$$w(N) = \frac{dZ(N)}{dt} \tag{23}$$

where Δt was set to 0.001 and N is the tracer number. As an example, one of the trajectories of virtual particles is shown in figures 10a and b. The orbit shows chaotic behavior. The glass in the furnace interchanges completely in approximately 20 h in the measurement. Figures 11a to d show the average histories of temperature and velocity for twenty glass particles obtained by monitoring them backward from the throat. The quality of glass is considered to be better if the average temperature near the throat is higher and the dispersion errors of temperature history and the average velocity are smaller. These numerical and experimental results are summarized in figure 12. The abscissa shows the average temperature and the ordinate indicates the standard deviation of the variation in temperature. Although the experimental data was obtained at the nozzle exit rather than at the throat, the glass melting involved almost no bubbles and glass fining was generated in case B1. The numerical results also showed a similar tendency. In case C2, the average temperature near the throat was high and the dispersion error of temperature history was relatively small. However, since the average velocity near the throat was faster, bubbles and nondissolved glass were mixed. According to the simulation results good-quality glass should be pulled, the temperature history was found to be stabilized near the throat and the temperature was found to be 1625 K or higher. These results are useful for determining the thermal parameters in order to design a real furnace.

5. Concluding remarks

We measured the velocity and temperature distributions in a glass melting furnace. The thermal flow in the furnace was investigated via the three-dimensional numerical simulation and the experimental measurement. First, we performed calculations on the basis of the boundary temperature obtained by the small furnace, and the numerical results were then compared to experimentally measured values. Next, in order to examine convection control, the electrode conditions of the lower heater, the effects of the heat loss through the walls and the batch slot were investigated. The numerical results were in good agreement with the measured values of the velocity and temperature distributions in the glass-melting furnace. We confirmed that the numerical simulation provides reliable results for the thermal flow in the melting furnace. We showed that the glass convection in the furnace can be controlled by changing the conditions of the lower heater and by taking advantage of the heat loss through the walls. Furthermore, the quality of glass products was evaluated by investigating the trajectory and temperature history of virtual glass particles. It became possible to understand the dominant flow and heat transportation phenomenon inside the furnace under difficult conditions by utilizing simultaneously the measurements of molten glass and the simulation results.

*

The present study was supported by a grant from New Energy and Industrial Technology Development Organization (NEDO) (Japan).

6. Nomenclature

6.1 Symbols

A_x,A_y	length of area of existence of a glass batch
C_p	specific heat at constant pressure
g	gravitational acceleration
K	overall heat loss coefficient
L_x, L_y, L_z	size of the small melting furnace
N	tracer number
n	refractive index
P	pressure
q	heat flux
$Q_1^{(k)}$	calorific value of the upper heater
Q_i	volumetric rate of Joule heat dissipation
r	distance
dS_1, dS_2	infinitesimal area
T	temperature
t	time
u, v, w	velocity components
U_{in}, U_{out}	inflow velocity,outflow velocity
V_h	area of cuboid
X, Y, Z	position of a virtual particle
x, y, z	coordinate components
X-Z, Y-Z	X-Z plane, Y-Z plane
β	thermal expansion coefficient
Δ	infinitesimal
γ	Stefan-Boltzmann constant
κ	thermal conductivity
μ	viscosity
ξ	normal direction to a wall
ϱ	density
σ	surface tension
ϕ_1, ϕ_2	angle
χ_R	mean absorption coefficient

6.2 Superscripts

(k)	index of the upper heater

6.3 Subscripts

a	ambient
bw	bottom wall
eff	effective
fw	front wall
h	heater
i	index of the lower heater
rad	radiation
R	Rosseland
rw	rear wall
s	glass batch interface
sw	sidewall
x, y, z	coordinates of the furnace
0	reference

7. References

[1] Viskanta, R. Review of three-dimensional mathematical modeling of glass melting. J. Non-Cryst. Solids **177** (1994) pp. 347–362.

[2] Ungan, A.; Viskanta, R.: Three-dimensional numerical modeling of circulation and heat transfer in a glass melting tank. Pt. 1. Mathematical formulation. Glastech. Ber. **60** (1987) no. 3, pp. 71–78.

[3] Ungan, A.; Viskanta, R.: Identification of the structure of the three-dimensional thermal flow in an idling container glass melter. Glass Technol. **28** (1987) no. 6, pp. 252–260.

[4] Choudhary, M. K.: A modeling study of flow and heat transfer in an electric melter, J. Non-Cryst. Solids 101 (1988) pp. 41–53.

[5] Choudhary, M. K.: Three-dimensional mathematical model for flow and heat transfer in electric glass furnaces. Heat Transfer Eng. **6** (1985) no. 4, pp. 55–65.

[6] Hayes, R. R.; Wang, J.; McQuay, W. M. et al.: Predicted and measured glass surface temperature in an industrial, regeneratively gas-fired flat glass furnace. Glastech. Ber. Glass Sci. Technol. **72** (1999) no. 12, pp. 367–377.

[7] Barklage-Hilgefort, H.; Mergler, K. W.; Voss, H.-J.: Strömungsmessungen im Läuterbereich einer rekuperativ beheitzten Glasschmelzwanne. Glastechn. Ber. **53** (1980) no. 2, pp. 27–36.

[8] Davies, D. H.; Davis, D. H.: How to get the most out of electric boosting. Pt. 1. Glass Ind. (1986) no. 3, pp. 21–24.

[9] Davies, D. H.; Davis, D. H.: How to get the most out of electric boosting. Pt. 2. Glass Ind. (1986) no. 4, pp. 22–30.

[10] Mori, U.; Hashima, H.; Konishi, A. et al.: Development of a method for measuring molten glass flow. Glass Technol. **43C** (2002) pp. 29–34.

[11] Hyre, M. R.; Paul, K.: Effect of natural convection and internal radiation on glass conditioning. In: Invited Papers: XIX International Congress on Glass, Edinburgh 2001. Sheffield: Society of Glass Technology, 2001. Pp. 259–265.

[12] Amsden, A. A.; Harlow, F. H.: Effect of natural convection and internal radiation on glass conditioning, J. Copm. Phys. **6** (1970) pp. 322–325.

[13] Lim, K. O.; Song, T. H.; Lee, K. S.: Patterns of natural convection driven by the free surface temperature distribution in a glass melting furnace, Glass Technol. **39**(1) (1998) pp. 27–31.

[14] Mazurin, O. V.; Streltsina, M. V.; Shvaiko-Shvaikovskaya, T. P.: Handbook of glass data. Pt. C. Ternary silicate glasses. Amsterdam (et al.): Elsevier, 1987. (Physical sciences data 15.)

[15] Neuroth, N.: Der Einfluß der Temperatur auf die spektrale Absorption von Gläsern im Ultraroten. Glastechn. Ber. (1952) no. 8, pp. 242–249.

E403P001

Contact:

Mr T. Hiejima
Research Associate
Department of Aerospace Engineering
Osaka Prefecture University
1-1 Gakuen-cho,
Sakai, Osaka, 599-8531
Japan
E-mail: hiejima@aero.osakafu-u.ac.jp